NASA TECHNICAL NOTE

NASA TN D-8390

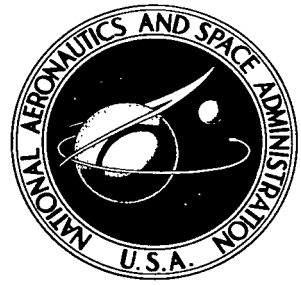

ANALYSIS OF DIFFERENTIAL ABSORPTION LIDAR TECHNIQUE FOR MEASUREMENTS OF ANHYDROUS HYDROGEN CHLORIDE FROM SOLID ROCKET MOTORS USING A DEUTERIUM FLUORIDE LASER

Clayton H. Bair and Frank Allario

Langley Research Center
Hampton, Va. 23665

NATIONAL AERONAUTICS AND SPACE ADMINISTRATION • WASHINGTON, D. C. • MAY 1977

1. Report No.	2. Government Accession No.	3. Recipient's Catalog No.
NASA TN D-8390		

4. Title and Subtitle
ANALYSIS OF DIFFERENTIAL ABSORPTION LIDAR TECHNIQUE FOR MEASUREMENTS OF ANHYDROUS HYDROGEN CHLORIDE FROM SOLID ROCKET MOTORS USING A DEUTERIUM FLUORIDE LASER

5. Report Date: May 1977

6. Performing Organization Code:

7. Author(s)
Clayton H. Bair and Frank Allario

8. Performing Organization Report No.: L-11144

9. Performing Organization Name and Address
NASA Langley Research Center
Hampton, VA 23665

10. Work Unit No.: 506-25-32-01

11. Contract or Grant No.:

12. Sponsoring Agency Name and Address
National Aeronautics and Space Administration
Washington, DC 20546

13. Type of Report and Period Covered: Technical Note

14. Sponsoring Agency Code:

15. Supplementary Notes

16. Abstract

The present study evaluates an active optical technique (differential absorption lidar (DIAL)) for detecting, ranging, and quantifying the concentration of anhydrous HCl contained in the ground cloud emitted by solid rocket motors (SRM). Results are presented of an experiment in which absorption coefficients of HCl were measured for several deuterium fluoride (DF) laser transitions demonstrating for the first time that a close overlap exists between the 2-1 P(3) vibrational transition of the DF laser and the 1-0 P(6) absorption line of HCl, with an absorption coefficient of 5.64 $(atm\text{-}cm)^{-1}$. These measurements show that the DF laser can be an appropriate radiation source for detecting HCl in a DIAL technique. Development of a mathematical computer model to predict the sensitivity of DIAL for detecting anhydrous HCl in the ground cloud is outlined, and results that assume a commercially available DF laser as the radiation source are presented. Elements of the computer model consist of a general development of the DIAL equations and calculations of the extinction and scattering coefficients used in the DIAL equations to estimate backscattered power. A multilayer diffusion model was used to predict cloud growth after stabilization in the atmosphere to obtain typical concentrations of molecular species in the cloud as a function of downwind distance from the launch pad for obtaining ranging information of the DIAL technique.

17. Key Words (Suggested by Author(s))	18. Distribution Statement
Laser DIAL technique Solid rocket motors Pollution detection	Unclassified – Unlimited Subject Category 45

19. Security Classif. (of this report)	20. Security Classif. (of this page)	21. No. of Pages	22. Price*
Unclassified	Unclassified	42	$4.00

*For sale by the National Technical Information Service, Springfield, Virginia 22161

ANALYSIS OF DIFFERENTIAL ABSORPTION LIDAR TECHNIQUE FOR MEASUREMENTS OF ANHYDROUS HYDROGEN CHLORIDE FROM SOLID ROCKET MOTORS USING A DEUTERIUM FLUORIDE LASER

Clayton H. Bair and Frank Allario
Langley Research Center

SUMMARY

The present study evaluates an active optical technique (differential absorption lidar (DIAL)) for detecting, ranging, and quantifying the concentration of anhydrous HCl contained in the ground cloud emitted by solid rocket motors (SRM). Results are presented of an experiment in which absorption coefficients of HCl were measured for several deuterium fluoride (DF) laser transitions demonstrating for the first time that a close overlap exists between the 2-1 P(3) vibrational transition of the DF laser and the 1-0 P(6) absorption line of HCl, with an absorption coefficient of 5.64 $(atm\text{-}cm)^{-1}$. These measurements show that the DF laser can be an appropriate radiation source for detecting HCl in a DIAL technique. Development of a mathematical computer model to predict the sensitivity of DIAL for detecting anhydrous HCl in the ground cloud is outlined, and results that assume a commercially available DF laser as the radiation source are presented. Elements of the computer model consist of a general development of the DIAL equations and calculations of the extinction and scattering coefficients used in the DIAL equations to estimate backscattered power. A multilayer diffusion model was used to predict cloud growth after stabilization in the atmosphere to obtain typical concentrations of molecular species in the cloud as a function of downwind distance from the launch pad for obtaining ranging information of the DIAL technique.

Results of a computer model which show the received laser power and signal-to-noise ratio as a function of range for both column content and range-resolved measurements for different particle size distribution for the Al_2O_3 particulates and H_2O aerosols in the ground cloud are presented. It was determined that column content measurements could be made for cloud distances 8 km from the launch pad with center-line concentrations of approximately 2 parts per million in a Gaussian cloud with a 1.5 km width by using a commercially available DF laser and conventional lidar instrumentation. Similarly, it was determined that range-resolved measurements could be performed with a lidar located 5 km from a Gaussian cloud which has stabilized in the manner described by the multilayered diffusion model.

INTRODUCTION

Background

The firing of large solid rocket motors for space shuttle boosters results in the generation of a ground cloud containing a combination of rocket combustion products mixed with atmospheric constituents. The composition of the ground cloud has been discussed in references 1 and 2, and among its constituents are included CO_2, H_2, H_2O, N_2, CO, HCl, and Al_2O_3. Because of the toxic and corrosive properties of anhydrous HCl and its acidic forms, it is desirable to understand the mechanisms of generation and depletion of anhydrous HCl in the cloud. This is especially important for understanding the dynamics of the chemistry of acid formation in the cloud if absorption of HCl by H_2O aerosols and Al_2O_3 particles is assumed. Also, for satisfying the environmental impact statement for the space shuttle program (July 1972) (ref. 3), the concentration of HCl in the ground cloud is an important parameter to be measured. Multilayer diffusion models that assess the potential ground-level toxic fuel hazard from rocket launches have been developed (ref. 4). These models apply meteorological data as input information and estimate ground level and cloud concentrations of the various constituents including HCl as a function of distance from the launch pad. Although these concentrations vary with the size of the rocket motor and the meteorological conditions, ground level and cloud concentrations of anhydrous HCl below 10 ppm are predicted after the cloud has stabilized.

The behavior of the ground cloud after the combustion products of the rocket have been released is discussed in reference 2. Cloud formation occurs rapidly by turbulent mixing of the combustion products with the atmosphere. Subsequently, the cloud rises to altitudes determined by atmospheric stability and rocket motor type (approximately 2750 to 3660 m for Titan IIIC), stabilizing at this altitude and drifting in a direction dictated by meteorological conditions. The actual size, shape, and range of the cloud are not simply characterized, but for a Titan IIIC rocket motor, a typical cloud diameter of 1 km is observed at a range 1 to 5 km from the launch pad. Ground-based in situ samplers suffer from the disadvantages that knowledge of the cloud drift direction must be known prior to launch for accurate placement of the samplers and frequent cloud passage over water requires seacraft whose operation may be limited by rough sea warnings. (See ref. 5.) From this information, it appears that a ground-based remote-sensing technique with range of 1 to 5 km is needed, capable of detecting concentrations of anhydrous HCl of 0.1 to 100 ppm with a spatial resolution of at least 150 m to obtain a three-dimensional map of the HCl concentration. (See ref. 6.)

Remote-Sensing Techniques

Passive optical remote measurements of anhydrous HCl in the ground cloud have been reviewed in references 5 and 6. Passive instruments perform measurements either in emission or absorption and require independent radiation sources such as the Sun or the thermally emitting hot gas in the cloud. In the emission mode, measurements are limited to that period of time when the cloud temperature is above ambient. In the absorption mode, solar radiation must be utilized; this condition requires either that the trajectory of the cloud be known prior to the measurement or that solar radiation scattered from cloud constituents be monitored. In either case, quantitative information of the HCl concentration in the cloud requires solution of complex radiative transfer equations. These limitations of passive techniques suggest consideration of active remote sensing techniques.

In this study, several active techniques were initially considered and included

(1) Raman scattering (RS)

(2) Resonance Raman scattering (RRS)

(3) Laser induced fluorescence (LIF)

(4) Differential absorption lidar (DIAL)

For the lower limits of concentration considered for our study (0.1 ppm at 5 km), it was concluded that only DIAL could provide the required sensitivity, specificity, and range required for the measurement. A comparative study of the active techniques has been performed in references 7 and 8. RS suffers from an extremely small scattering coefficient; thus, this technique is limited to ranges less than 1 km. RRS which should increase the magnitude of the scattering cross section has not been demonstrated for HCl and requires operation of lasers in the ultraviolet (UV) where atmospheric scattering and extinction are severe. LIF of HCl in the UV or infrared (IR) has not been demonstrated and although a potentially larger cross section than RS exists, the problem of quenching by collisions with foreign gases restricts the quantitative information that can be derived from a fluorescence measurement.

DIAL Technique

Differential absorption lidar has been suggested and demonstrated by several authors as an active ranging technique for detecting ambient concentrations of molecules such as H_2O, NO_2, CO, and SO_2 by using visible and UV lasers. (See refs. 9 to 15.) One version of the DIAL technique applied to the detection of HCl in a solid rocket motor (SRM) ground cloud is illustrated in figure 1. Two laser pulses are transmitted to the pollutant cloud, each pulse sequentially displaced in time from the other by time interval $\Delta\tau$. Some of the laser photons penetrate the cloud and are backscattered by

Al_2O_3 particles and H_2O aerosols in the cloud to the laser receiver. One pulse has a wavelength (λ^{on}) overlapping one of the vibrational-rotational absorption lines of the 3.5-μm band of HCl. The second pulse has a wavelength (λ^{off}) which falls in between the absorption lines of HCl but sufficiently close to λ^{on} to account for signal changes in the backscattered signal due to changes in backscattering. Photons at λ^{off} will not be absorbed by HCl, but serve as a reference signal for the backscattering coefficient. For this application of DIAL, a reference signal λ^{off} is extremely important since the volume backscattering is primarily produced by the distribution of large particles in the cloud (Mie scattering). The Mie scattering coefficient and distribution of particles currently are not well known empirically. Therefore, any changes in backscattering due to Al_2O_3 particles and H_2O aerosols in the cloud must be carefully monitored by a reference signal.

In this paper, results of the study to evaluate the application of DIAL to detecting anhydrous HCl in SRM ground clouds are presented. Absorption coefficients of HCl obtained by using a deuterium fluoride (DF) laser as the radiation source are summarized. Demonstration that the DF laser is a suitable radiation source for this problem is important since the DF laser has demonstrated high energy (>1 joule/pulse) and is commercially available for immediate application to a field experiment with slight modification. The development of a mathematical computer model to predict the applicability of DIAL to detection of anhydrous HCl is presented. The concentration and spatial distribution of ground cloud constituents as a function of time are described by a multilayer diffusion model. Empirical data are used to obtain analytically the apparent index of refraction of the cloud due to the H_2O aerosols and Al_2O_3 particles emitted by the rocket motor. The variation of laser signal return and S/N ratio for a variety of cloud conditions is presented, including specific limitations imposed on the DIAL technique by large concentrations of H_2O aerosols in the cloud. The analytical studies are summarized and recommendations for implementing this technique at on-site rocket launches are made.

SYMBOLS

A	lidar receiver telescope area
a_n, b_n	Mie complex scattering coefficients
c	speed of light
Δf	detector bandwidth
$i_1(x,m,\theta)$	first Mie angular dependent intensity function

$i_2(x,m,\theta)$ second Mie angular dependent intensity function

$K_{abs}(r,\lambda,m)$ Mie absorption efficiency factor

$K_{ext}(r,\lambda,m)$ Mie extinction efficiency factor

$K_{sca}(r,\lambda,m)$ Mie scattering efficiency factor

k absorption coefficient

$k(R)$ extinction coefficient due to all aerosol and molecular constituents other than pollutant

k_{calc} calculated absorption coefficient

k_{exp} experimental absorption coefficient

$k_{ext}(\lambda,m)$ aerosol extinction coefficient

$k_p(R)$ pollutant absorption

m aerosol index of refraction

NEP noise equivalent power

N_o particle number density

$N_p(R)$ pollutant concentration at a distance R from lidar

$N_p\left(R_i + \frac{\Delta R}{2}\right)$ average pollutant concentration in ith range cell

ΔN difference between total burden measurements made at successive range cells

$n(r)$ particle size distribution function

P_i any returned power term in retrieval concentration expressions

ΔP_i uncertainty (noise) associated with P_i

P_o output laser power

P_r backscattered power returned to lidar receiver

P_r^{off} backscattered power returned to lidar receiver at reference wavelength

P_r^{on} backscattered power returned to lidar receiver at signal wavelength

$P_r^{on}(i), P_r^{off}(i)$ backscattered power returned to lidar receiver at reference and signal wavelengths, respectively, from ith range cell

p_t total pressure

Re( ) real part

R_i distance from lidar to ith range cell

ΔR size of range cell

r particle radius

$S_1(x,m,\theta)$ first Mie complex amplitude function

$S_2(x,m,\theta)$ second Mie complex amplitude function

S/N signal-to-noise ratio

X retrieved concentration interpreted as signal in signal-to-noise expression

ΔX noise associated with retrieved concentration

x Mie size parameter

$\beta(R)$ total backscatter coefficient from a volume element a distance R from lidar

$\beta(\theta = 180^o), \beta_{180}$ volume backscatter coefficient

η optical efficiency

λ DF laser wavelength

$\bar{\nu}$ HCl absorption line frequency

$\bar{\nu}_1, \bar{\nu}_2$ DF laser frequencies

π_n functions related to Legendre polynomials and their derivatives used in Mie calculations

ρ Al_2O_3 or H_2O mass density

ρ_o aerosol mass concentration

$\sigma_{abs}(r,\lambda,m)$ aerosol absorption cross section

$\sigma_{ext}(r,\lambda,m)$ aerosol extinction cross section

σ_p^{on} pollutant absorption cross section

$\sigma_{sca}(r,\lambda,m)$ aerosol scattering cross section

τ laser pulse length

τ_n functions related to Legendre polynomials and their derivatives used in Mie calculations

$\Delta\tau$ time interval between successive laser pulses

Superscripts:

on refers to frequency overlapping absorption line

off refers to frequency not overlapping absorption line

Subscripts:

max maximum

min minimum

MEASUREMENTS OF HCl ABSORPTION COEFFICIENTS

A primary requirement for implementation of the DIAL technique for atmospheric pollution sensing is the availability of a high energy pulsed laser source with a wavelength overlapping a vibrational-rotational transition of the molecule to be detected. HCl has a fundamental absorption band at 3.5 μm, and potential laser sources for DIAL are the optical parametric oscillator (OPO), the HCl laser, and the DF laser. For early implementation of the DIAL technique, only the DF laser has demonstrated sufficient energy per pulse for ranging capabilities beyond 1 km.

By comparing published DF laser transitions (refs. 16 and 17) with published values of HCl absorption line parameters (ref. 18), it appeared that several strong overlaps existed within the spectral region of the HCl fundamental. In order to verify the degree of overlap and to obtain accurate values of the HCl absorption coefficients for these DF laser transitions, an experiment was performed which demonstrated for the first time that a strong overlap exists between the 2-1 P(3) vibrational transition of DF and the 1-0 P(6) absorption line of HCl^{37}. The measured absorption coefficient was 5.64 $(atm\text{-}cm)^{-1}$. By measuring the absorption coefficient as a function of pressure (ref. 19), the 2-1 P(3) transition of DF was estimated to lie within 1.32 GHz of the center of the HCl^{37} transition. The measured absorption coefficient was used in subsequent DIAL calculations to estimate performance of this technique for detecting HCl in the exhaust of the SRM.

A schematic of the instrumentation used to measure absorption coefficients of HCl with a DF laser is shown in figure 2. A commercial line tunable DF laser operating in the fundamental transverse mode was used. Several characteristics of the laser are given subsequently. When operating with DF as the active medium, 24 laser lines were observed that ranged in vibrational transitions from 4-3 to 1-0 and covered the spectrum from 3.493 to 4.100 μm. Most DF lines exhibited energies $\geqq$50 mJ/pulse with a measured optical pulse width at the half intensity point of 500 ns. Maximum pulse energies were obtained at a repetition rate $\leqq$0.5 Hz. The laser emission of the DF laser was observed to be superradiant even with the use of a line selection grating. Single wavelength operation was obtained by using a 0.3-m spectrograph as an optical filter. As indicated in figure 2, the laser output was focused by a lens system onto the entrance slit of the spectrograph. The output of the spectrograph was collimated with a CaF_2 lens, and then divided into a sapphire beam splitter. Reference detector B was used to monitor amplitude fluctuations of the laser; signal detector A was used to monitor the intensity of the laser beam transmitting through the gas cell. The absorption cell was made of Pyrex with sapphire windows. The cell length was nominally 1 m. Premix concentrations of HCl and N_2 at a total pressure of 1 atm were used. Two mixtures with 0.27

and 10.2 percent HCl were used. These concentrations were dictated by the availability of the mixtures.

The reference and signal detectors, A and B, respectively, were pyroelectric detectors with focusing lenses. To process the optical signals at a 0.5-Hz repetition frequency and to suppress the effect of amplitude fluctuations in the laser, a two-channel gated integrator detection system was employed. A schematic of the instrumentation is shown in figure 2. Briefly, the output of each detector was sampled by a gated integrator and fed to an A/B ratio unit. The output of the ratio unit could be displayed directly as an analog signal or converted to a digital signal with an analog-to-digital converter (ADC) and recorded by a line printer. Typically, the digitized technique was used where, for each measurement, 100 laser shots were recorded; data corresponding to obvious misfirings of the laser were discarded. The mean and standard deviations for each set of measurements were computed. Typically, uncertainty of the reported data is better than ±5 percent and is primarily due to the amplitude fluctuations exhibited by the laser. The linearity of the detection system was also checked over the range from 1 to 100 mJ by comparing the energy of the laser recorded by the pyroelectric detectors with a calibrated thermopile.

Prior to performing the measurements, a theoretical computer program was used to identify the potential overlap of the 24 DF laser lines with HCl absorption lines for conditions simulating absorption through a 1-m cell for the HCl-N_2 mixtures used in the experiment. For these calculations, values of DF laser transitions were obtained from the literature (refs. 16 and 18). Spectroscopic parameters for HCl were taken from reference 18 with a Voigt profile used to describe line shapes. Calculations of HCl absorption coefficients included wing effects from lines up to 22 cm^{-1} from the line center.

A summary of the theoretical and experimental results is shown in table 1. The first two columns identify the DF transitions which potentially showed the strongest overlap. The third and fourth columns list the experimentally measured absorption coefficient (k_{exp}) and the calculated absorption coefficient (k_{calc}) in $(atm\text{-}cm)^{-1}$, respectively, for a 10.2-percent mixture of HCl in N_2. The fifth and sixth columns list similar data for a 0.27-percent mixture. The difference in the calculated values for the two mixtures is due to self-broadening effects. In the latter case because of the low concentration of HCl, only the 2-1 P(3) transition showed significant absorption in the experiment as predicted by the computer model. Other DF lines not listed in table 1 (19 lines) were examined for potential overlap with the 10.2-percent mixtures, but no overlaps were identified. The result is again in agreement with the predictions of the computer model. The agreement between the calculated and experimental absorption coefficients is very good. The data listed in table 1 indicated that the most likely candidate for λ^{on} in a remote sensing lidar measurement is the 2-1 P(3) DF laser line, since it has the largest

absorption coefficient. However, if this line is too strongly absorbed, the 2-1 P(4) DF laser line would provide a very good alternative for λ^{on}. In the subsequent computer analysis, the 2-1 P(3) transition will be used as λ^{on} for all the cases considered.

Another parameter which can readily be obtained from this experiment is the separation between the 2-1 P(3) DF transition and the HCl^{37} absorption line. An experiment of this type and the results obtained are described in detail in reference 20. Figure 3 shows results of the experiment in which a mixture containing 2 torr of HCl and 758 torr of N_2 was reduced in pressure in steps to obtain the dependence of absorption coefficient $(atm\text{-}cm)^{-1}$ on total pressure. The circles represent the experimental points. The top solid curve is the predicted dependence for a DF laser frequency, $\bar{\nu}_1 = 2750.09\ cm^{-1}$ (ref. 16), and the bottom solid curve is the predicted dependence for $\bar{\nu}_2 = 2750.05\ cm^{-1}$ (ref. 17), by assuming that the line position of the HCl^{37} absorption line is at $\bar{\nu}(1\text{-}0\ P(6)) = 2750.13\ cm^{-1}$. As shown in reference 20, which also includes effects due to pressure shifting of the absorption line, the relative position of the DF laser frequency to the absorption line is 1.32 ± 0.15 GHz. This result is in good agreement with the separation obtained by assuming the 2-1 P(3) DF transition and 1-0 P(6) HCl line position given, respectively, by Long, et al. (ref. 16) and Benedict, et al. (ref. 18).

COMPUTER MODEL DEVELOPMENT

In this section, the computer code developed to evaluate the feasibility of the DIAL technique for measuring concentrations of HCl in the ground cloud of the solid rocket motors (SRM) is outlined. The DIAL equation (ref. 14) applied to this problem is discussed for range-resolved measurements of HCl from the edge of the cloud to some range R_i into the cloud. Calculations of the extinction and scattering coefficients used in the DIAL equation to estimate molecular concentrations and backscattered power are outlined. Elements of a multilayer diffusion model to describe the distribution of cloud constituents spatially and with changing time are then discussed (ref. 4).

DIAL Equations

The DIAL equation applied to the problem of detecting molecular constituents in a localized cloud with a uniformly mixed distribution has been discussed in reference 14 for CO and NO_2. In this work, the scatterers were assumed to be Rayleigh and Mie scatterers in a natural atmosphere. For detection of anhydrous HCl in the ground cloud of an SRM, a more complex calculation is required to account for the complex composition of the cloud (HCl, Al_2O_3, and H_2O), its change in composition with time as the cloud diffuses away from the launch pad, and the change of composition as the leading edge of the cloud is penetrated.

In general, the returned power P_r from a range cell located a distance R_1 from the laser transmitter and receiver is given by

$$P_r = \frac{P_o \eta A}{R_1^2} \Delta R \, \beta(R_1) \, e^{-2\int_0^{R_1} k(R)+k_p(R)\, dR} \tag{1}$$

where η is the optical efficiency of the receiver telescope, A is the area of the telescope, P_o is the output power of the laser at the transmitter, $\Delta R = c\tau/2$ is the length of range cell, c is the speed of light, τ is the length of the laser pulse, and $\beta(R)$ is the backscatter coefficient including Rayleigh and Mie scattering from all constituents within the range cell ΔR. The extinction coefficient $k(R)$ includes extinction from molecular and aerosol constituents other than the pollutant to be detected up to range R_1; $k_p(R)$ includes molecular absorption due to pollutant within the laser path up to range R_1. The designations for ΔR and R_1 are noted in figure 1.

In the DIAL technique, two wavelengths are chosen with a wavelength on the absorption line λ^{on} giving rise to an absorption coefficient $k_p^{on}(R)$, and with a wavelength off the absorption line λ^{off} giving rise to an absorption coefficient $k_p^{off}(R)$. By choosing the proper DF transition, $k_p^{off}(R) \approx 0$. If it is assumed that k_p is the only wavelength-dependent term in equation (1), then the ratio of backscattered power at the two wavelengths is given by

$$\frac{P_r^{off}}{P_r^{on}} = e^{2\int_0^{R_1} k_p^{on}(R)\, dR} \tag{2}$$

Since $\sigma_p^{on} N_p(R) = k_p^{on}(R)$ where $N_p(R)$ is the concentration of the molecule (cm^{-3}) and σ_p^{on} is the absorption cross section of the on wavelength, then

$$\int_0^{R_1} N_p(R)\, dR = \frac{1}{2\sigma_p^{on}} \log_e \frac{P_r^{off}}{P_r^{on}} \tag{3}$$

where the integral represents the total concentration of absorbing molecules from the edge of the cloud to a range R_1 in the cloud. For a uniformly mixed cloud with scatterers only in the natural atmosphere, equation (3) can be used directly to obtain results as in reference 14. For the ground cloud problem, appropriate values of $k(R)$ and $\beta(R)$ must be evaluated. The methodology for calculating realistic values for $k(R)$ and $\beta(R)$ is given in the section "Computer Model Development."

For obtaining range-resolved measurements of HCl in the cloud (for example, a nonuniformly mixed cloud), the difference between the successive total burden measurements is found. Range-resolved measurements are generated by incrementing the penetration distance of total burden measurements into the cloud by steps of ΔR. Then equation (3) can be used to obtain the column content from the edge of the cloud to R_2 where $R_2 = R_1 + \Delta R$. In this case equation (3) becomes

$$\int_0^{R_2} N_p(R)\, dR = \frac{1}{2\sigma_p^{on}} \log_e \left[\frac{P_r^{off}(2)}{P_r^{on}(2)}\right] \tag{4}$$

The difference between total burden measurements ΔN is given as

$$\Delta N = \int_0^{R_2} N_p(R)\, dR - \int_0^{R_1} N_p(R)\, dR = \frac{1}{2\sigma_p^{on}} \left\{ \log_e \left[\frac{P_r^{off}(2)}{P_r^{on}(2)}\right] - \log_e \left[\frac{P_r^{off}(1)}{P_r^{on}(1)}\right] \right\} \tag{5}$$

or

$$\Delta N = \int_{R_1}^{R_1+\Delta R} N_p(R)\, dR = \frac{1}{2\sigma_p^{on}} \log_e \left[\frac{P_r^{off}(2)}{P_r^{on}(2)} \frac{P_r^{on}(1)}{P_r^{off}(1)}\right] \tag{6}$$

where $P_r^{off}(1)$ and $P_r^{on}(1)$ refer to power measurements at R_1, and $P_r^{off}(2)$ and $P_r^{on}(2)$ refer to power measurements at R_2. Assuming that $N_p(R)$ is constant across the range cell ΔR leads to the following expression:

$$N_p\left(R_1 + \frac{\Delta R}{2}\right) = \frac{1}{2\Delta R \sigma_p^{on}} \log_e \left[\frac{P_r^{off}(2)}{P_r^{on}(2)} \frac{P_r^{on}(1)}{P_r^{off}(1)}\right] \tag{7}$$

By varying the position of range cell 2 with respect to the leading edge of the cloud, a spatial profile of the HCl concentration from the edge of the cloud to a penetration distance R_1 into the cloud can be obtained.

The signal-to-noise (S/N) ratio of the backscattered signal has been calculated as one of the output parameters of the computer code. In the 3.5-μm region where HCl has its fundamental absorption band, indium antimonide (InSb) is an appropriate detector. Reference 14 has adequately treated the noise terms in DIAL systems in the infrared.

According to reference 14, an infrared detector is dark current or background limited. The noise term ΔX is given by

$$(\Delta X)^2 = \sum_i \left(\frac{\partial X}{\partial P_i}\right)^2 (\Delta P_i)^2 \tag{8}$$

where X is the signal given by either equation (3) or (7) ($i = 2$ for column content measurements and $i = 4$ for range-resolved measurements) and $\Delta P_i = NEP\sqrt{\Delta f}$ independent of P_i where NEP represents the noise equivalent power and Δf is the bandwidth. With the expression for noise given, the S/N becomes

$$\frac{S}{N} = \frac{X}{\Delta X} = \frac{\log_e \left[\frac{P_r^{off}(1)}{P_r^{on}(1)}\right]}{NEP\sqrt{\Delta f}\left\{\left[\frac{1}{P_r^{off}(1)}\right]^2 + \left[\frac{1}{P_r^{on}(1)}\right]^2\right\}^{1/2}} \tag{8a}$$

for column content measurements and

$$\frac{S}{N} = \frac{X}{\Delta X} = \frac{\log_e \left[\frac{P_r^{off}(2)}{P_r^{on}(2)} \frac{P_r^{on}(1)}{P_r^{off}(1)}\right]}{NEP\sqrt{\Delta f}\left\{\left[\frac{1}{P_r^{off}(2)}\right]^2 + \left[\frac{1}{P_r^{on}(2)}\right]^2 + \left[\frac{1}{P_r^{off}(1)}\right]^2 + \left[\frac{1}{P_r^{on}(1)}\right]^2\right\}^{1/2}} \tag{8b}$$

for range-resolved measurements.

An error analysis for the DIAL technique has been published by Schotland (ref. 21) in which he has included uncertainties in the measurements associated with the absorption coefficient, atmospheric parameters, and jitter in laser frequency. A similar analysis should be performed for this problem, but the uncertainty in composition of the particle scatterers and uncertainty of condition in the ground cloud currently make this type of analysis difficult to apply. In the application to detection of H_2O in the atmosphere, Schotland found that primary sources of uncertainty were uncertainties associated with the laser frequency, and that noise associated with the signal limited the accuracy at higher altitudes.

Calculation of Extinction and Backscattering Coefficients

The absorption and scattering mechanisms considered in this work for the incident DF radiation are shown schematically in figure 4. Absorption and scattering of λ^{on} and λ^{off} by the natural atmosphere were included over a range extending from the lidar transmitter through the cloud. Absorption and scattering of the laser radiation by Al_2O_3 particles, H_2O aerosols, and HCl molecules were assumed to be confined within the exhaust cloud.

Molecular absorption due to natural atmospheric constituents and HCl from 2500 cm^{-1} to 2900 cm^{-1} was computed by using a computer code developed by Seals (ref. 22). Line parameter data were obtained from the AFCRL data tape compilation (ref. 23) for the major absorbers in this region: H_2O, O_3, N_2O, CH_4, and CO_2. Similar data were obtained for HCl from reference 18. A Voigt profile was generally used in the calculations and wing effects were included up to 25 cm^{-1} from the center of the DF laser line. Continuum absorption due to N_2 and H_2O was included.

Results of the calculated atmospheric absorption coefficients for several DF laser lines considered as potential wavelengths are shown in table 2, together with some results of calculations performed by Long (ref. 16) and measurements made by Spencer (ref. 24). The absorption coefficients due to Spencer listed in the table include a calculated contribution from the N_2 and H_2O continua.

In order to calculate the contribution to the extinction and backscatter due to H_2O aerosols and Al_2O_3 particles, the complex index of refraction and particle size distribution must be known at the wavelengths of the transmitting laser radiation. Since at 3.5 μm the laser wavelength and particle size are approximately the same, Mie theory must be employed instead of small particle scattering (Rayleigh) or the geometric optics approximations. From Mie theory (refs. 25 and 26), the extinction coefficient (cm^{-1}) for a system of particles of different radii characterized by a size distribution $n(r)$ in particles/cm^3-μm is given by

$$k_{ext}(\lambda,m) = \int_0^\infty n(r)\ \sigma_{ext}(r,\lambda,m)\ dr \tag{9a}$$

where $\sigma_{ext}(r,\lambda,m)$ is the extinction cross section of a particle of radius r. As is indicated, σ_{ext} is a function of λ and m, where m, the index of refraction, is also dependent on λ. Expressions similar to equation (9a) for absorption and scattering coefficients of aerosols and particulates can also be written.

In order to calculate k_{ext} from Mie theory, it is first necessary to define the efficiency factor $K_{ext}(r,\lambda,m)$ where

$$K_{ext}(r,\lambda,m) \equiv \frac{\sigma_{ext}(r,\lambda,m)}{\pi r^2} = \frac{2}{x^2} \sum_{n=1}^{\infty} (2n + 1)\mathrm{Re}\left(a_n + b_n\right) \tag{9b}$$

Similar expressions for the scattering and absorption efficiency factors are given as

$$K_{sca}(r,\lambda,m) \equiv \frac{\sigma_{sca}(r,\lambda,m)}{nr^2} = \frac{2}{x^2} \sum_{n=1}^{\infty} (2n + 1)\left(\left|a_n\right|^2 + \left|b_n\right|^2\right) \tag{9c}$$

$$K_{abs}(r,\lambda,m) \equiv \frac{\sigma_{abs}(r,\lambda,m)}{\pi r^2} = K_{ext}(r,\lambda,m) - K_{sca}(r,\lambda,m) \tag{9d}$$

In equations (9a) to (9d), m is the complex index of refraction, $x = 2\pi r/\lambda$ is the Mie size parameter for a particle of radius r and for incident radiation at wavelength λ. Re( ) indicates that the real part of the sum, $a_n + b_n$ of the Mie complex scattering coefficients is to be taken. The complex scattering coefficients a_n and b_n can be expressed as Bessel functions of the first and third kind and their derivatives. Values for K_{ext}, K_{sca}, and K_{abs} were calculated according to a technique suggested by Kattawar and Plass (ref. 27).

Another parameter that must be calculated for the DIAL equation is the volume backscattering coefficient $\beta(R)$ which was calculated from the angular dependent intensity functions i_1 and i_2 defined by

$$i_1(x,m,\theta) = S_1(x,m,\theta)\, S_1{}^*(x,m,\theta) \tag{10}$$

$$i_2(x,m,\theta) = S_2(x,m,\theta)\, S_2{}^*(x,m,\theta) \tag{11}$$

where

$$S_1(x,m,\theta) = \sum_{n=1}^{\infty} \frac{2n + 1}{n(n + 1)} \left(a_n \pi_n + b_n \tau_n\right) \tag{12a}$$

$$S_2(x,m,\theta) = \sum_{n=1}^{\infty} \frac{2n + 1}{n(n + 1)} \left(b_n \pi_n + a_n \tau_n\right) \tag{12b}$$

and the asterisk indicates the complex conjugate.

In equations (12a) and (12b), π_n and τ_n are functions related to the Legendre polynomials and their derivatives. Their exact dependence is given in reference 25. The volume backscattering coefficient at $\theta = 180^o$ for a specified particle size distribution and for a specified scatterer is given by

$$\beta(\theta = 180^o) = \int_0^\infty \frac{\lambda^2}{4\pi^2}\left(\frac{i_1 + i_2}{2}\right) n(r)\, dr \tag{13}$$

where i_1 and i_2 were calculated at $\theta = 180^o$. The backscattering coefficient $\beta(R)$ used in equation (1) was calculated by adding contributions from the three scatterers, Al_2O_3, H_2O, and naturally occurring particulates in the atmosphere.

Values of the extinction and backscattering coefficients were calculated on a CDC 6600 computer for the five DF laser wavelengths listed in table 1. For Al_2O_3, four different particle size distributions were calculated, designated I to IV. Particle size distributions labeled I, II, and III were taken from the literature (refs. 28, 29, and 30, respectively) as suggested particle size distributions for relatively small rocket motors. Distribution IV was obtained from reference 31 by applying the fitted curve of recent experimental measurements (ref. 32) of particle size against rocket motor size to the Titan IIIC nozzle. In table 3, pertinent data for the various size distributions used in the calculations are shown. The first column lists the designation and appropriate reference; the second column lists the distribution function; the third and fourth columns list the minimum and maximum radii assumed for the integration points, respectively; the fifth column lists the ratio of the mass concentration to the particle number density ρ_o/N_o given by

$$\frac{\rho_o}{N_o} = \frac{4\pi\rho}{3} \frac{\int_0^\infty r^3 n(r)\, dr}{\int_0^\infty n(r)\, dr} \times 10^{-3} \tag{14}$$

where ρ, the mass density of Al_2O_3, was taken to be 3.7 g/cm^3. The leading constants in the distribution functions listed in the second column have been normalized so that $\rho_o = 1$ mg/m^3. The listing in the fifth column is a convenient way to convert from literature values given in mass density to number densities. In table 4, the values of k_{ext} and β_{180} for the four Al_2O_3 distribution functions for the five pertinent DF laser transitions are given and were used in the DIAL equation to evaluate backscattered power and S/N ratio. For the Al_2O_3 particulates, the index of refraction was taken from Bauer and Carlson (ref. 29).

A procedure similar to that used for Al_2O_3 was used to obtain the contribution to k_{ext} and $\beta(R)$ for the H_2O aerosols. The index of refraction for H_2O aerosols was taken from Centeno (ref. 33). The particle size distributions marked "Cloud" and "Haze M" by Deirmendjian (ref. 34) were used to describe H_2O aerosol size distribution; these two models were chosen to give results representative of two vastly different particulate sizes.

For the natural aerosols in the atmosphere, the indices of refraction and the size distribution were taken from McClatchey (ref. 35). In table 5, k_{ext} and $\beta(R)$ for the H_2O aerosols and atmospheric aerosols are given.

Multilayer Diffusion Model

The computer model discussed and the experimental results obtained were used to evaluate the feasibility of DIAL for detecting HCl in the ground cloud of solid rocket motors. The parameters used to describe the ground cloud are based on results of the multilayer diffusion model (ref. 4) developed to predict cloud growth after stabilization based on initial cloud dimensions and existing meteorological conditions. In general, the model assumes diffusion of a Gaussian plume with provisions made for vertical mixing and depletion due to gravitational settling and precipitation. Figure 5 shows some preliminary results from this model which have been used to provide estimates of cloud growth and composition as a function of range for use in the computer code for the DIAL calculations. The data have been obtained by assuming a Titan IIIC launch vehicle during a sea breeze condition. Figure 6 shows the width of the Gaussian cloud (measured from the two points at which the total mass concentration is 10 percent of the center-line concentration). Typical cloud dimensions vary from <1.2 km at 1.0 km from point of stabilization to >20 km at 14 km after stabilization.

Figure 5 shows the predicted decrease in the concentrations of the three cloud constituents considered important in this study, Al_2O_3 aerosols, H_2O aerosols, and anhydrous HCl, as a function of downwind distance from the point of stabilization. The relative mass concentrations are based on the fuel properties characteristic of the Titan IIIC launch vehicle and are not dependent on the size distributions chosen for the aerosols. If the actual number density is required, equation (14) can be used with ρ and ρ_o chosen appropriately to Al_2O_3 or H_2O depending upon the constituents desired.

RESULTS

In order to evaluate the feasibility of the DIAL technique, the computer code discussed was used to obtain two types of information. First is the received power at the receiver as a function of range for the two DIAL wavelengths, λ^{off} and λ^{on}. (See eq. (1).) Second is the S/N for the received signal as a function of range for both

column content and range-resolved measurements given by equations (8a) and (8b), respectively. Center-line concentrations of HCl, Al_2O_3 particulates, and H_2O aerosols for the Gaussian cloud were varied as a function of downwind distance as previously discussed. Four Al_2O_3 and two H_2O particle size distributions were also considered. The assumed parameters of the lidar system are summarized in table 6.

Figure 7(a) shows typical results of the returned power (μW) as a function of range (km) for the "on," 2-1 P(3), and "off," 1-0 P(7), wavelengths for a cloud 2 km downwind. The laser transmitter is located at zero and the edge of the cloud at 1.35 km. The center-line concentrations and cloud width were taken from figures 5 and 6, respectively, with particulate size distributions given by model IV for the Al_2O_3 particulates and cloud for the H_2O aerosols. The decrease of the returned signal before the cloud is encountered is due to the $1/R^2$ dependence, as well as to atmospheric extinction. The signal difference that can be observed immediately before cloud penetration is a result of a differential in atmospheric attenuation (see table 2) and will give a (negative) contribution to the retrieved HCl concentration. The sharp increase of returned signal at 1.35 km is due to the enhanced backscatter from the cloud particulates. After cloud penetration, the returned power increases until extinction (exponential in particulate concentration) dominates backscatter (linear in particulate concentration). Inside the cloud, the 2-1 P(3) laser line is attenuated faster than the 1-0 P(7) line because of the presence of HCl which gives a signal difference that can be related to the HCl concentration by equation (4) for column content or equation (7) for range-resolved measurements.

In figure 7(b), the S/N ratio defined by equation (8) is plotted as a function of penetration depth into the cloud. The squares represent the total burden measurements and the circles represent range-resolved measurements with a 75-m range resolution. These results indicate that for a Gaussian cloud, 2-km downwind range resolved measurements can be made up to 700 m into the cloud with a $S/N > 10$.

Figures 8(a) and 8(b) are similar to figure 7 with the exception that haze M was used to describe the H_2O aerosols. Since haze M heavily weights submicron particles, approximately 1200 times more particles had to be included than in Deirmendjian's cloud model to give the same mass density as required by figure 5. In spite of the increased number of H_2O aerosols, a comparison of figures 8 and 7 shows only a slight decrease in returned power and S/N as a function of range.

The effect of small Al_2O_3 particles is shown in figures 9 and 10, which employ the Al_2O_3 model I size distribution and are otherwise identical to figures 7 and 8, respectively. As mentioned previously, the number density of Al_2O_3 particulates is adjusted to give the mass concentration required by the multilayer diffusion model. (See fig. 5.) Although the values of returned power and S/N are lower than the large Al_2O_3 particle

case (Al_2O_3 model IV), range-resolved information can still be achieved with S/N > 10 up to 600 m into the cloud.

In figures 7 to 10 the capability of making a measurement on a cloud that is located 2 km from the launch site is examined; however, as the cloud continues to drift downwind, its size and composition change. Figures 11 and 12 indicate the effect that this downwind drift would have on the measurement capability of a stationary lidar located at the launch site. In figure 11 the maximum S/N for a total burden measurement is shown as a function of downwind distance, where the H_2O aerosols are described by the cloud model. The separate curves correspond to the four Al_2O_3 particle size distributions as indicated in the figure. As shown by the figure, column content measurements can be made on clouds up to 8 km downwind for the small Al_2O_3 particle case and on clouds up to 14 km downwind for the larger particles expected for exhaust engines in the Titan IIIC class. Figure 12 is similar to figure 11 with the exception that haze M is used to describe the H_2O aerosols. As before, the greatly reduced H_2O particle size only slightly reduces the S/N. In all cases in figures 11 and 12 the penetration depth at which the S/N maximizes varies from approximately 300 m near the launch site to approximately 1 km for downwind distances exceeding 8 km. Results similar to those shown in figures 11 and 12 show that range-resolved measurements can be performed on clouds from up to 5 km downwind for Al_2O_3 model I and up to 8 km downwind for Al_2O_3 model IV. The maximum S/N occurs at approximately the same penetration depth as for column content measurements.

CONCLUDING REMARKS

A computer model has been developed which has shown that using an experimentally measured absorption coefficient of HCl at the 2-1 P(3) DF laser wavelength and conservative laser-receiver lidar parameters, HCl can be detected in the SRM tropospheric ground cloud. Several particulate size distributions were considered for both H_2O and Al_2O_3 aerosols. In all the cases considered, it was determined that range-resolved and column content measurements could be made on clouds up to 5 to 8 km, respectively, from the launch pad with center-line concentrations $\approx$2 ppm and width $\approx$1.5 km. Penetration depths of at least 500 m could be achieved with profiling information available every 75 m. The downwind range at which useful information could be obtained in this lidar simulation was limited not by lack of differential signal but rather by lack of total returned signal. Therefore, a higher energy laser and/or larger telescope receiver would increase the measurement capability over the system considered here. Also, an alternative to the stationary lidar considered in this study could be an aircraft-based lidar capable of fol-

lowing the ground cloud and therefore restricting the $1/R^2$ total power losses characteristic of the lidar signal returned from distance R.

Langley Research Center
National Aeronautics and Space Administration
Hampton, VA 23665
December 22, 1976

REFERENCES

1. Cesta, Ramon P.; and McLoth, Malcolm E.: Launch Conditions Produced by the Titan III-C Launch Vehicle. Amer. Indust. Hygeine Assn. J., vol. 30, no. 6, Nov.-Dec. 1969, pp. 635-639.

2. Study of Solid Rocket Motors for a Space Shuttle Booster. Appendix E – Environmental Impact Statement Solid Rocket Motor Space Shuttle Booster. UTC 4205-72-7 (Contract NAS 8-28431), United Technology Center, Mar. 15, 1972. (Available as NASA CR-123626.)

3. Environmental Statement for the Space Shuttle Program – Final Statement. NASA, July 1972.

4. Dumbauld, R. K.; Bjorklund, J. R.; and Bowers, J. F.: NASA/MSFC Multilayer Diffusion Models and Computer Program for Operational Prediction of Toxic Fuel Hazards. NASA CR-129006, 1973.

5. Gregory, Gerald L.; and Storey, Richard W., Jr.: Effluent Sampling of Titan III C Vehicle Exhaust. NASA TM X-3228, 1975.

6. Zwick, H.; Ward, V.; and Beaudette, L.: Feasibility Study of the Application of Existing Techniques To Remotely Monitor Hydrochloric Acid in the Atmosphere. TR 73-226A, Barringer Res. Ltd., Apr. 1973. (Available as NASA CR-112274.)

7. Bartle, E. Roy; Meckstroth, Edgar A.; and Kaye, Sam: Development of HCl and HF Detection System. AFRPL TR-71-59, U.S. Air Force, June 1971. (Available from DDC as AD 884 193.)

8. Measures, R. M.: A Comparative Study of Laser Methods of Air Pollution Mapping. UTIAS Rep. No. 174, Univ. of Toronto, Dec. 1971.

9. Kildal, Helge; and Byer, Robert L.: Comparison of Laser Methods for the Remote Detection of Atmospheric Pollutants. Proceedings of IEEE, vol. 59, no. 12, Dec. 1971, pp. 1644-1663.

10. Schotland, R. M.: Some Observations of the Vertical Profile of Water Vapor by Means of a Laser Optical Radar. Proceedings of the Fourth Symposium on Remote Sensing of Environment, Rev. ed., 4864-11-X, Willow Run Lab., Inst. Sci. & Technol., Univ. of Michigan, Dec. 1966, pp. 273-283.

11. Grant, W. B.; Hake, R. D., Jr.; Liston, E. M.; Robbins, R. C.; and Proctor, E. K., Jr.: Calibrated Remote Measurement of NO_2 Using the Differential-Absorption Backscatter Technique. Appl. Phys. Lett., vol. 24, no. 11, June 1, 1974, pp. 550-552.

12. Henningsen, T.; Garbuny, M.; and Byer, R. L.: Remote Detection of CO by Parametric Tunable Laser. Appl. Phys. Lett., vol. 24, no. 5, Mar. 1, 1974, pp. 242-244.

13. Ahmed, Samir A.: Molecular Air Pollution Monitoring by Dye Laser Measurement of Differential Absorption of Atmospheric Elastic Backscatter. Appl. Opt., vol. 12, no. 4, Apr. 1973, pp. 901-903.

14. Byer, Robert L.; and Garbuny, Max: Pollutant Detection by Absorption Using Mie Scattering and Topographic Targets as Retroreflectors. Appl. Opt., vol. 12, no. 7, July 1973, pp. 1496-1505.

15. Hoell, James M., Jr.; Wade, William R.; and Thompson, R. T., Jr.: Remote Sensing of Atmospheric SO_2 Using the Differential Absorption Lidar Technique. International Conference on Environmental Sensing and Assessment, Vol. 1 (Las Vegas, Nevada), Sept. 1975.

16. Long, R. K.; Hills, F. S.; and Trusty, G. L.: Calculated Absorption Coefficients for DF Laser Frequencies. RADC-TR-73-389, U.S. Air Force, Nov. 1973. (Available from DDC as AD 775 373.)

17. Deutsch, Thomas F.: Molecular Laser Action in Hydrogen and Deuterium Halides. Appl. Phys. Lett., vol. 10, no. 8, Apr. 15, 1967, pp. 234-236.

18. Benedict, William S.; Herman, Robert; Moore, Gordon E.; and Silverman, Shirleigh: The Strengths, Widths, and Shapes of Infrared Lines. II. The HCl Fundamental. Canadian J. Phys., vol. 34, no. 8, Aug. 1956, pp. 850-875.

19. Allario, Frank; and Seals, R. K., Jr.: Measurements of NH_3 Absorption Coefficients With a $C^{13}O_2^{16}$ Laser. Appl. Opt., vol. 14, no. 9, Sept. 1975, pp. 2229-2233.

20. Bair, C. H.; and Allario, F.: Measurement of HCl Absorption Coefficients With a DF Laser. Appl. Opt., vol. 16, no. 1, Jan. 1977, pp. 97-100.

21. Schotland, Richard M.: Errors in the Lidar Measurement of Atmospheric Gases by Differential Absorption. J. Appl. Meteorol., vol. 13, no. 1, Feb. 1974, pp. 71-77.

22. Seals, R. K., Jr.: Atmospheric Windows for HF Laser Radiation Between 2.7μ and 3.2μ. Appl. Opt., vol. 11, no. 12, Dec. 1972, pp. 2979-2980.

23. McClatchey, R. A.; Benedict, N. S.; Clough, S. A.; Burch, D. E.; Calfee, R. F.; Fox, K.; Rothman, L. S.; and Garing, J. S.: AFCRL Atmospheric Absorption Line Parameters Compilation. AFCRL-TR-73-0096, U.S. Air Force, Jan. 1973. (Available from DDC as AD 762 904.)

24. Spencer, D. J.; Denault, G. C.; and Takimoto, H. H.: Atmospheric Gas Absorption at DF Laser Wavelengths. Appl. Opt., vol. 13, no. 12, Dec. 1974, pp. 2855-2868.

25. Van de Hulst, H. C.: Light Scattering by Small Particles. John Wiley & Sons, Inc., c.1957.

26. Deirmendjian, D.; Clasen, R.; and Viezee, W.: Mie Scattering With Complex Index of Refraction. J. Opt. Soc. America, vol. 51, no. 6, June 1961, pp. 620-633.

27. Kattawar, George W.; and Plass, Gilbert N.: Electromagnetic Scattering From Absorbing Spheres. Appl. Opt., vol. 6, no. 8, Aug. 1967, pp. 1377-1406.

28. High Energy Solid Propellant Combustion Efficiency Investigation. AFRPL TR-66-42, U.S. Air Force, Apr. 1966. (Available from DDC as AD 371 483.)

29. Bauer, Ernest; and Carlson, Donald J.: Mie Scattering Calculations for Micron Size Alumina and Magnesia Spheres. J. Quant. Spectrosc. Radiat. Transfer, vol. 4, no. 3, May-June 1964, pp. 363-374.

30. Laderman, A. J.; Kuby, W. C.; Byron, S. R.; Carlson, D. J.; and Bartky, C. D.: Study of Thermal Radiation, Particle Impingement Heating, and Flow Field Analysis of Solid Propellant Rocket Exhausts. Publ. No. U-4045 (Contract NAS 8-20276), Aeronutron Div., Philco-Ford Corp., Apr. 19, 1964. (Available as NASA CR-85466.)

31. Worster, Bruce W.; and Kadomiya, Ronald H.: Rocket Exhaust Aluminum Oxide Particle Properties. Tech. Rep. ARI RR-30, Aerodyne Research, Inc., Aug. 1973. (Available from DDC as AD 913 363.)

32. Delaney, I. J.; Radke, H. H.; and Smith, P.: Exhaust Particle Size Data From Small and Large Solid Rocket Motors. TOR-1001/S2951-18/-3, Aerospace Corp., July 1967. (Available from DDC as AD 847 672.)

33. Centeno, Melchor V.: The Refractive Index of Liquid Water in the Near Infra-Red Spectrum. J. Opt. Soc. America, vol. 31, no. 3, Mar. 1941, pp. 244-247.

34. Deirmendjian, D.: Scattering and Polarization Properties of Water Clouds and Hazes in the Visible and Infrared. Appl. Opt., vol. 3, no. 2, Feb. 1964, pp. 187-196.

35. McClatchey, Robert A.; and Selby, John E. A.: Atmospheric Attenuation of Laser Radiation From 0.76 to 31.25 μm. AFCRL-TR-74-0003, U.S. Air Force, Jan. 1974.

TABLE 1.- MEASURED k_{exp} AND CALCULATED k_{calc} ABSORPTION COEFFICIENTS IN $atm^{-1}cm^{-1}$ OF HCl FOR FIVE DF LASER LINES

DF transition		10.2% HCl in N_2		0.27% HCl in N_2	
$\bar{\nu}$, cm^{-1}	Identification	k_{exp}	k_{calc}	k_{exp}	k_{calc}
2839.78	1-0 P(3)	0.067	0.049	---	0.039
2816.38	1-0 P(4)	.031	.024	---	.020
2750.09	2-1 P(3)	----	5.00	5.64	5.46
2727.30	2-1 P(4)	.22	.176	---	.142
2703.99	2-1 P(5)	.020	.017	---	.014

TABLE 2.- ATMOSPHERIC ABSORPTION COEFFICIENTS AT SEVERAL DF LASER WAVELENGTHS

Transition	Long		Spencer		Present study	
	$\bar{\nu}$, cm^{-1}	k_{calc}, km^{-1}	$\bar{\nu}$, cm^{-1}	k_{exp}, km^{-1} (a)	$\bar{\nu}$, cm^{-1}	k_{calc}, km^{-1}
1-0 P(3)	2839.78	0.1032	-----	----	2839.78	0.1196
1-0 P(4)	2816.38	.1044	-----	----	2816.38	.1062
[b]2-1 P(3)	2750.09	.04079	2750.0	0.039	2750.09	.04071
[b]1-0 P(7)	2743.00	.06019	2743.0	.058	2743.00	.05929
2-1 P(4)	2727.30	.06773	2727.4	.050	2727.30	.07217
2-1 P(5)	2703.99	.02846	2703.9	.033	2703.99	.02862

[a]Absorption coefficients listed in this column include a calculated contribution for the N_2 and H_2O continua.

[b]The 2-1 P(3) and 1-0 P(7) transitions were used as λ^{on} and λ^{off}, respectively, in the DIAL calculations.

TABLE 3.- DESCRIPTION OF THE Al_2O_3 AEROSOL MODELS USED IN THIS STUDY

Designation and reference	Distribution function	r_{min}, μm	r_{max}, μm	$\frac{\rho_o/N_o, mg/m^3}{particle/cm^3}$
I (ref. 28)	$1115r^2e^{-2.4r^3}$	0.01	2	0.006456
II (ref. 29)	$342.7r^{0.5}e^{-2.5r}$	.01	6	.01302
III (ref. 30)	$48.04re^{-1.78r}$	.01	10	.06595
IV (ref. 31)	$1.920e^{-0.65r}$	.01	20	.3385

TABLE 4.- EXTINCTION COEFFICIENTS $\left(km^{-1}/mg/m^3\right)$ AND BACKSCATTER COEFFICIENTS $\left(km^{-1}sr^{-1}/mg/m^3\right)$ FOR THE FOUR Al_2O_3 PARTICLE SIZE DISTRIBUTIONS CONSIDERED IN THIS STUDY

$\bar{\nu}$, cm^{-1}	Al_2O_3 model I		Al_2O_3 model II		Al_2O_3 model III		Al_2O_3 model IV	
	k_{ext}	β_{180}	k_{ext}	β_{180}	k_{ext}	β_{180}	k_{ext}	β_{180}
2839.78	0.2707	0.003950	0.4015	0.02210	0.2756	0.03532	0.1164	0.03526
2816.38	.2656	.003906	.3999	.02166	.2758	.03479	.1165	.03493
2750.09	.2440	.003707	.3918	.01945	.2766	.03242	.1172	.03335
2743.00	.2426	.003676	.3913	.01932	.2767	.03224	.1172	.03318
2727.30	.2390	.003670	.3899	.01903	.2768	.03199	.1173	.03308
2703.99	.2341	.003635	.3880	.01863	.2770	.03149	.1176	.03278

TABLE 5.- EXTINCTION COEFFICIENTS AND BACKSCATTER COEFFICIENTS FOR NATURALLY OCCURRING AEROSOLS AND TWO H_2O AEROSOL MODELS

$\bar{\nu}$, cm^{-1}	Natural aerosols*		Cloud†		Haze M†	
	k_{ext}	β_{180}	k_{ext}	β_{180}	k_{ext}	β_{180}
2839.78	7.115×10^{-6}	1.367×10^{-7}	0.3106	6.225×10^{-3}	0.7711	1.016×10^{-2}
2816.38	7.050	1.355	.3119	6.325	.7358	9.709×10^{-3}
2750.09	6.868	1.338	.3164	7.100	.6552	8.840
2743.00	6.845	1.335	.3169	7.130	.6497	8.782
2727.30	6.787	1.333	.3183	7.138	.6303	8.507
2703.99	6.716	1.327	.3205	7.154	.5943	7.998

*Extinction coefficients and backscatter coefficients given in $km^{-1}/particle/cm^3$ and $km^{-1}sr^{-1}/particle/cm^3$, respectively.

†Extinction coefficients and backscatter coefficients given in $km^{-1}/mg/m^3$ and $km^{-1}sr^{-1}/mg/m^3$, respectively.

TABLE 6.- LASER/RECEIVER PARAMETERS USED IN THE DIAL CALCULATIONS

Laser:

λ^{on}	2-1 P(3) DF laser line
λ^{off}	1-0 P(7) DF laser line
Laser output, mJ	100
Pulse width, ns	500

Receiver:

NEP, $W\text{-}Hz^{-1/2}$	3×10^{-12}
Detector area, cm^2	0.01
Telescope area, cm^2	1000
Range gate, m	75
Optical efficiency	0.1

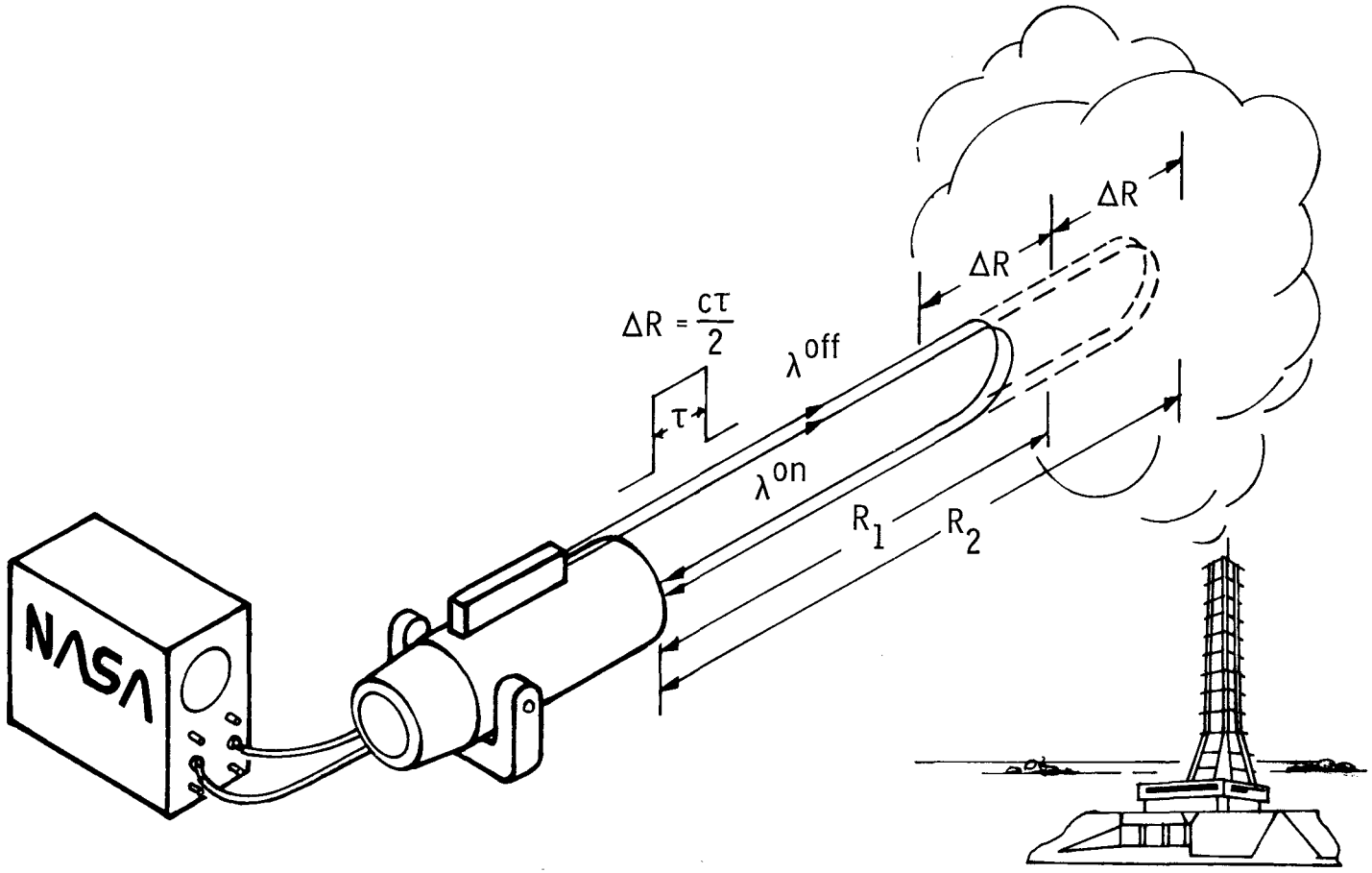

Figure 1.- Schematic of a two laser wavelength DIAL measurement applied to the detection of HCl in an SRM ground cloud.

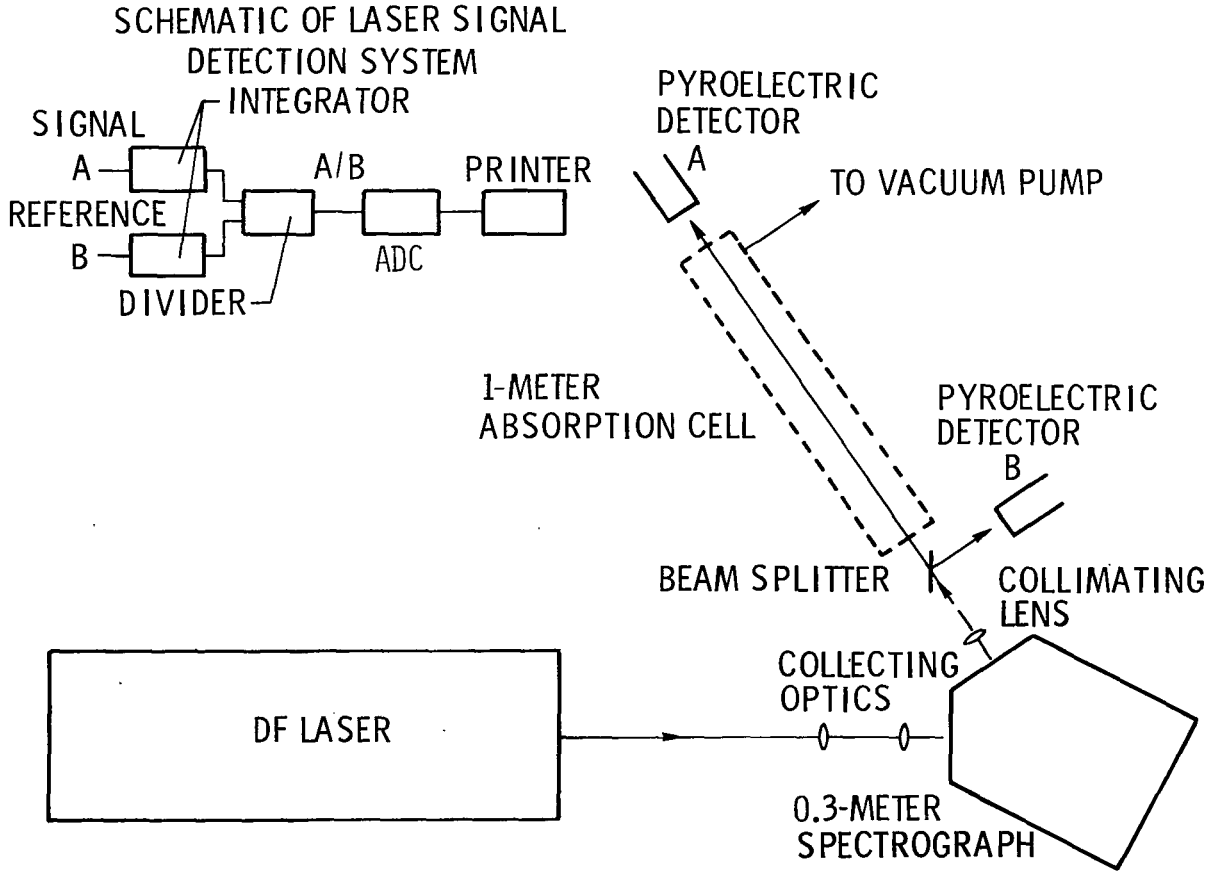

Figure 2.- Schematic of the HCl absorption experiment and the laser signal detection system used to measure overlap between HCl absorption lines and DF laser lines.

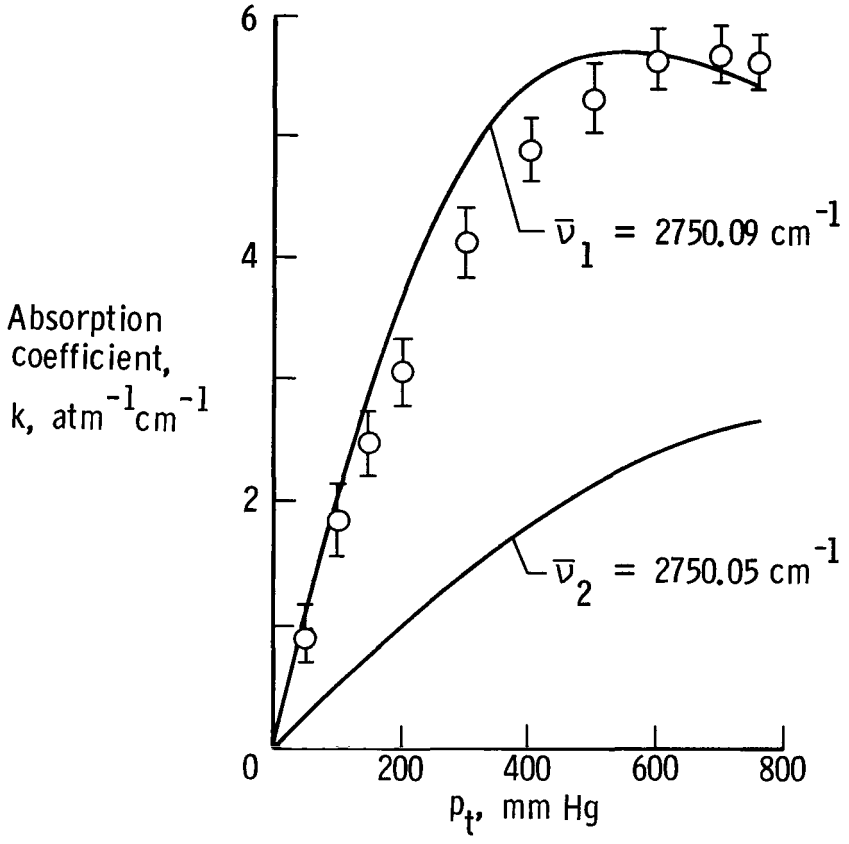

Figure 3.- Variation of the absorption coefficient k with total pressure p_t for a 0.27-percent mixture of HCl in N_2.

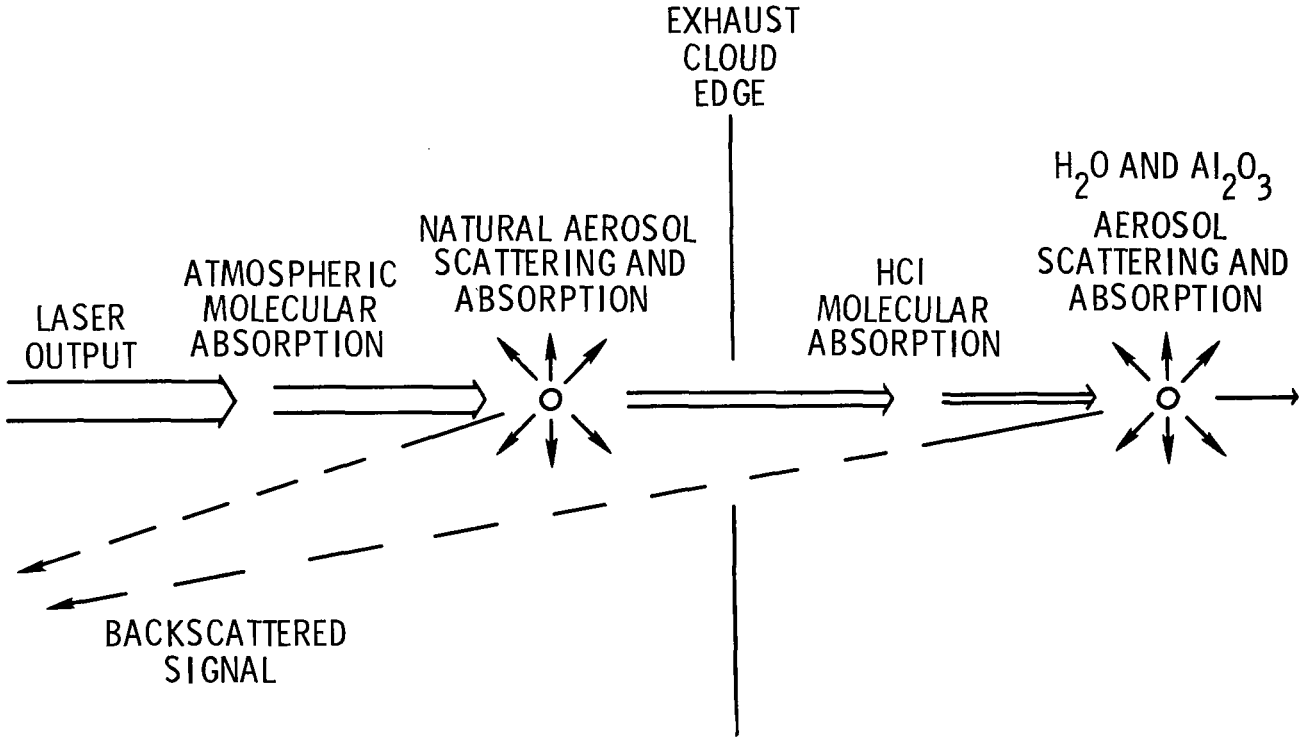

Figure 4.- Extinction mechanisms considered important in the computer model for measuring HCl in rocket exhaust cloud.

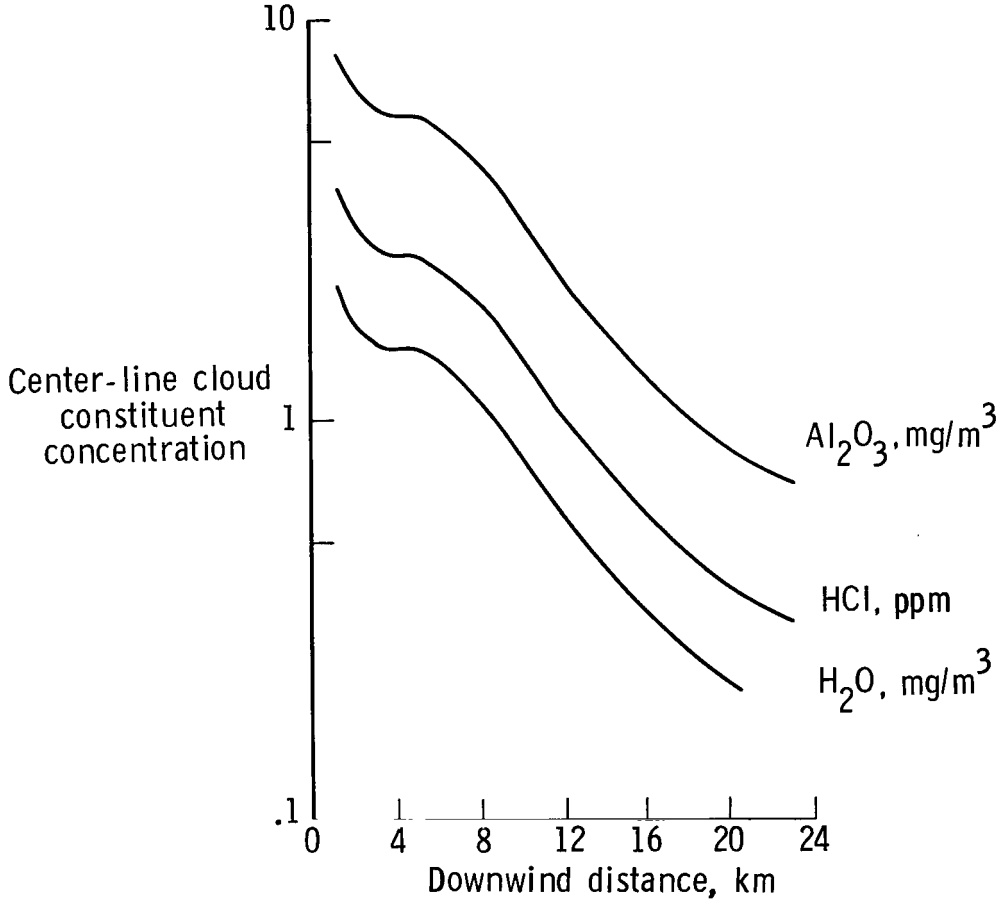

Figure 5.- Center-line concentrations for Al_2O_3 and H_2O aerosols and anhydrous HCl as a function of downwind distance for a normal Titan IIIC launch during a sea breeze regime at Kennedy Space Center.

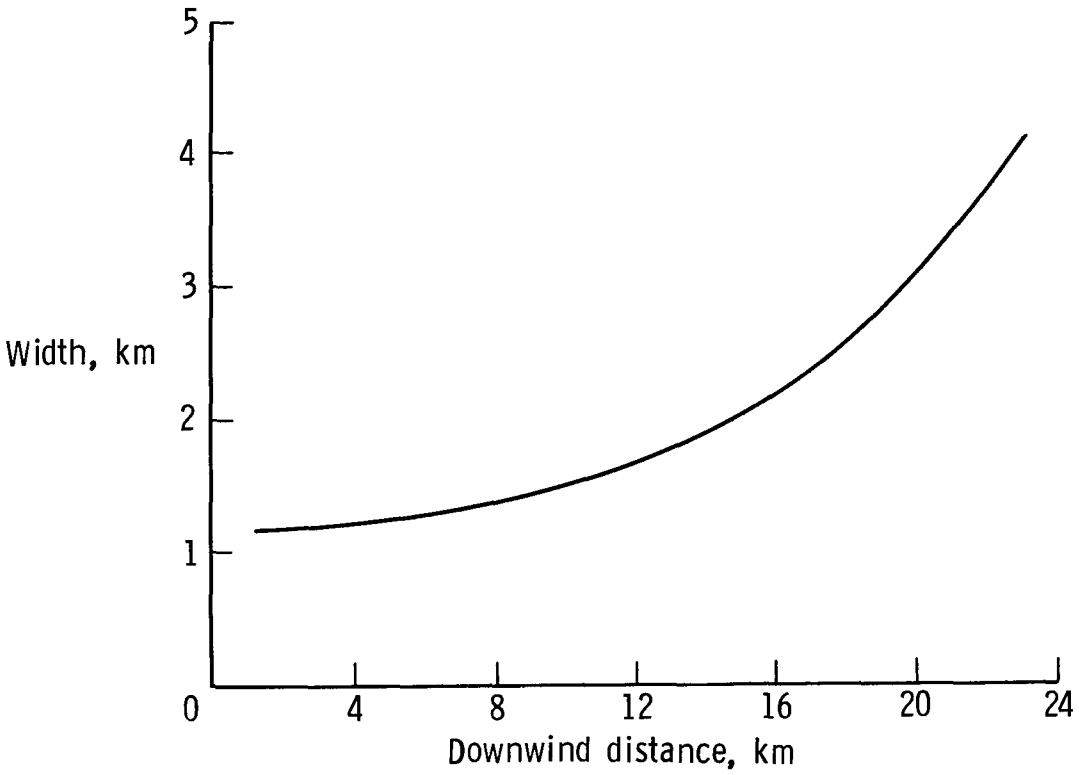

Figure 6.- Predicted cloud width as a function of downwind distance for a typical Titan IIIC launch.

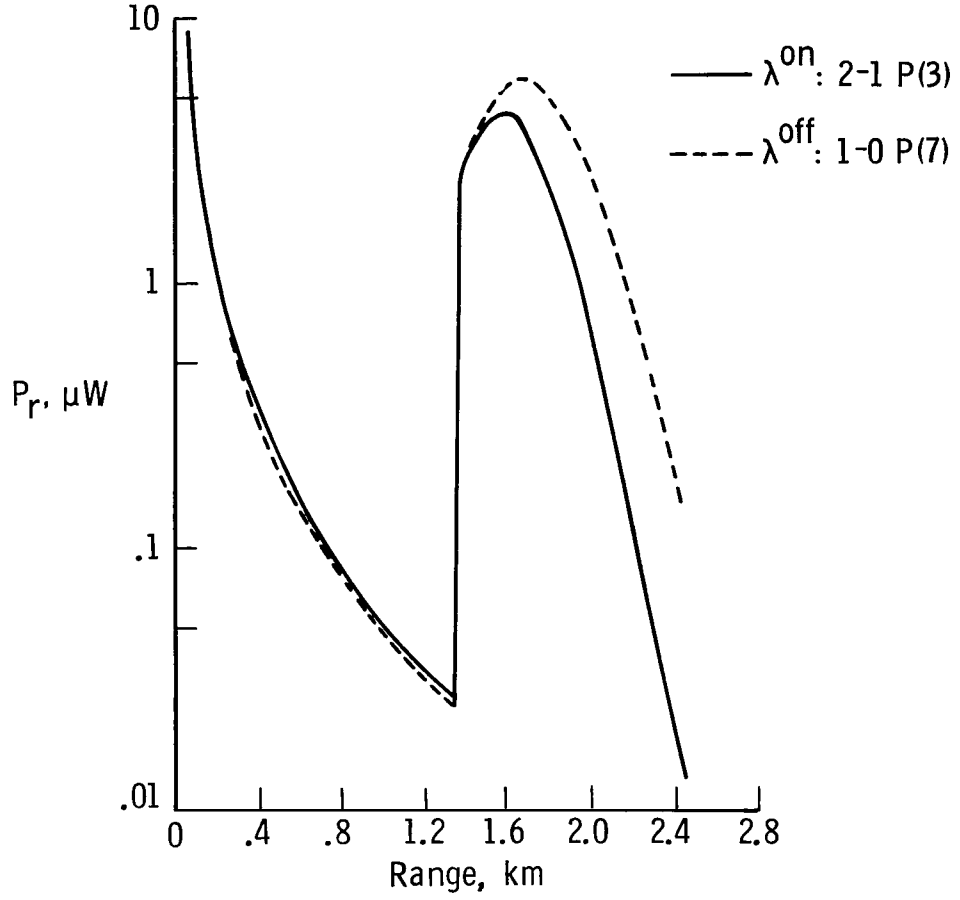

(a) Signal returns as a function of range from lidar package.

Figure 7.- Calculated signal returns and signal-to-noise ratios for a cloud located 2 km downwind using Al_2O_3 model IV and H_2O model cloud.

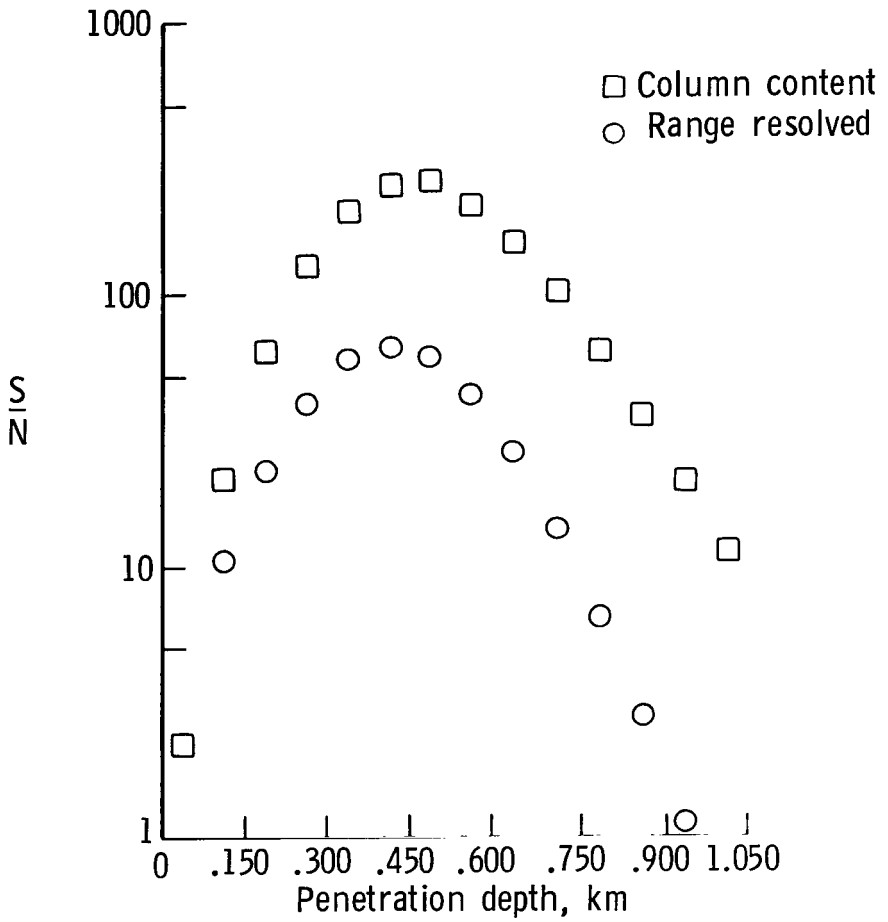

(b) Signal-to-noise ratios as a function of penetration depth.

Figure 7.- Concluded.

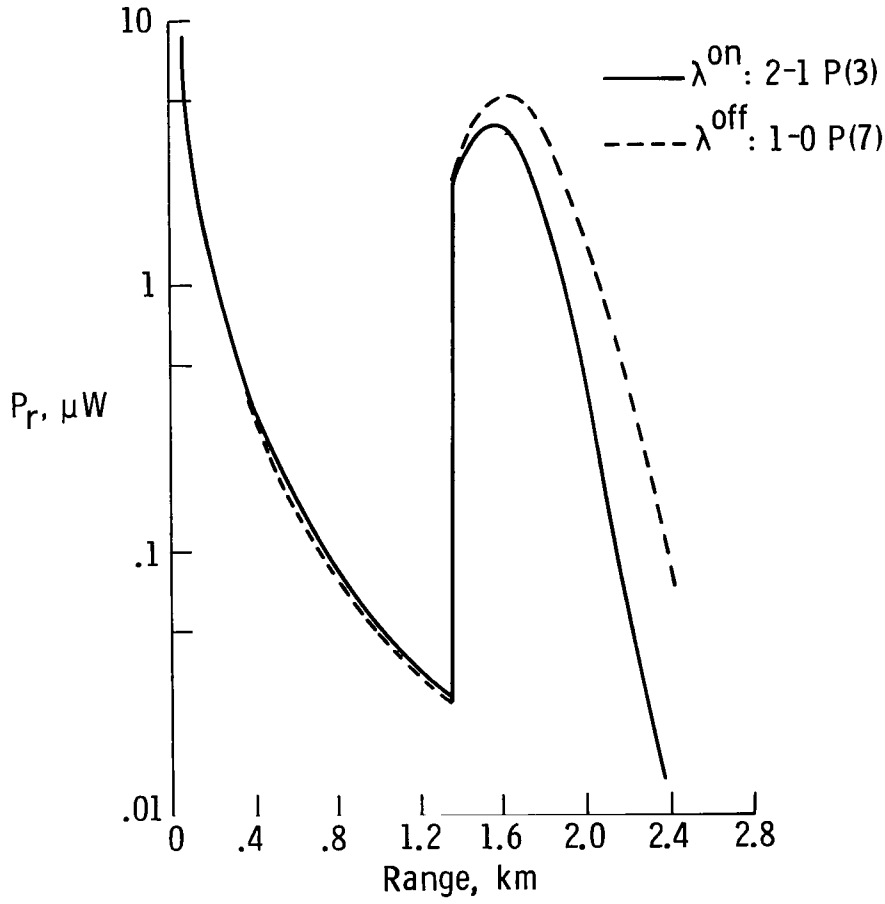

(a) Signal returns as a function of range from lidar package.

Figure 8.- Calculated signal returns and signal-to-noise ratios for a cloud located 2 km downwind using Al_2O_3 model IV and H_2O model haze M.

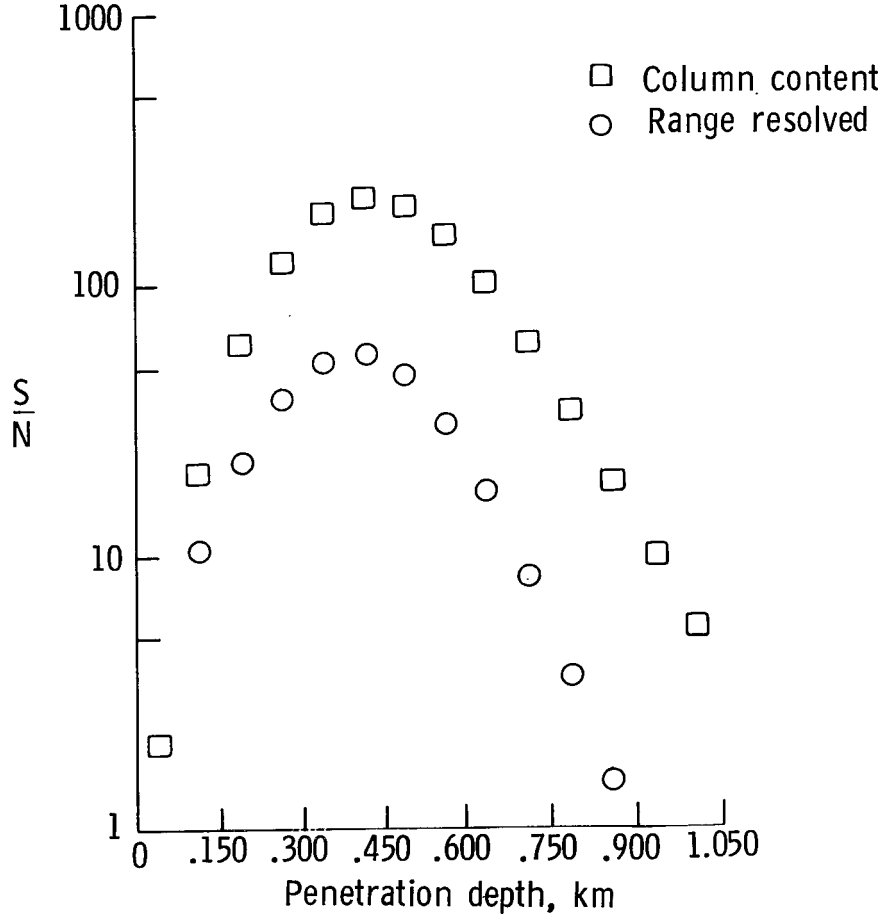

(b) Signal-to-noise ratios as a function of penetration depth.

Figure 8.- Concluded.

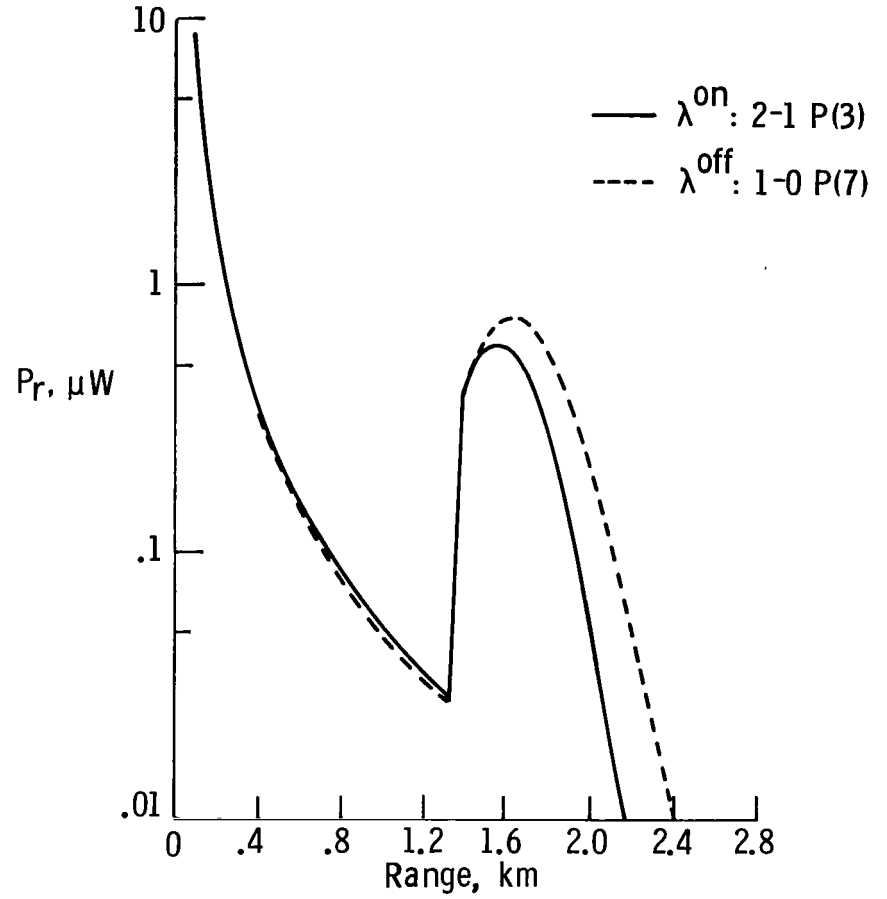

(a) Signal returns as a function of range from lidar package.

Figure 9.- Calculated signal returns and signal-to-noise ratios for a cloud located 2 km downwind using Al_2O_3 model I and H_2O model cloud.

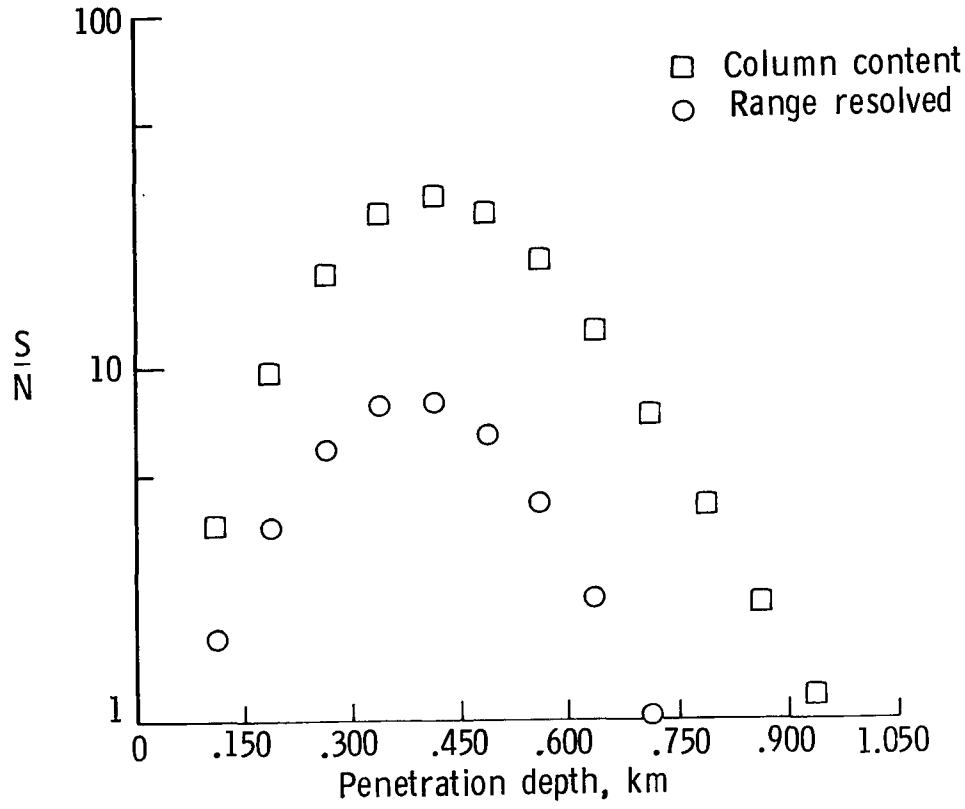

(b) Signal-to-noise ratios as a function of penetration depth.

Figure 9.- Concluded.

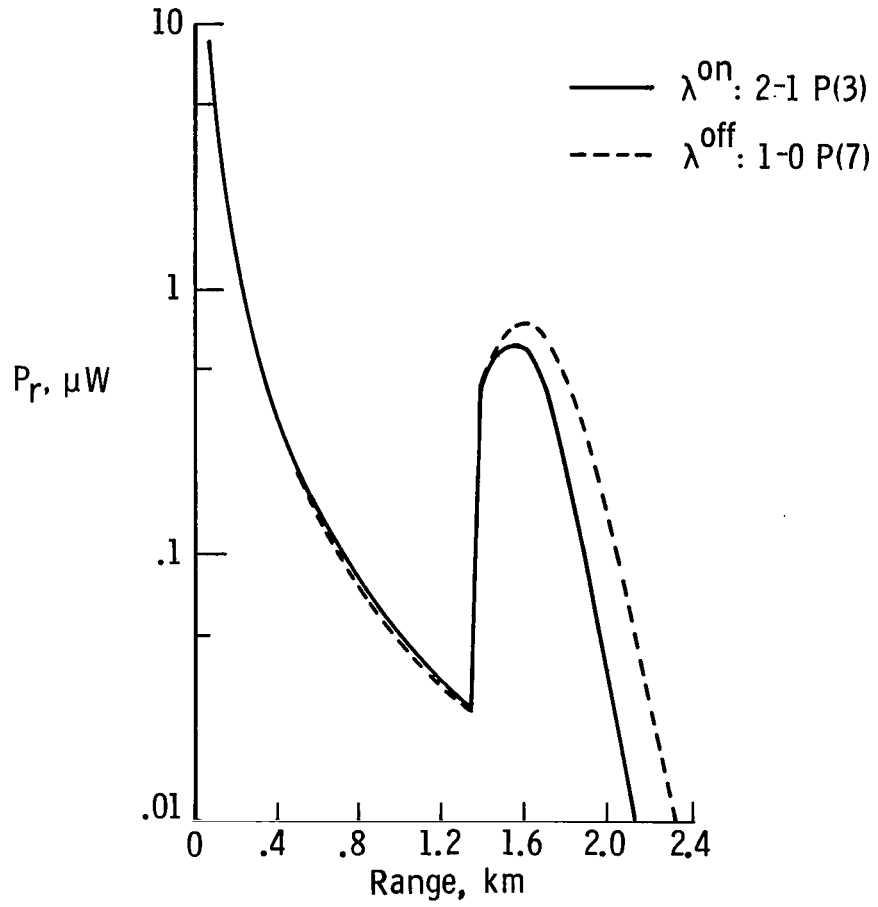

(a) Signal returns as a function of range from lidar package.

Figure 10.- Calculated signal returns and signal-to-noise ratios for a cloud located 2 km downwind using Al_2O_3 model I and H_2O model haze M.

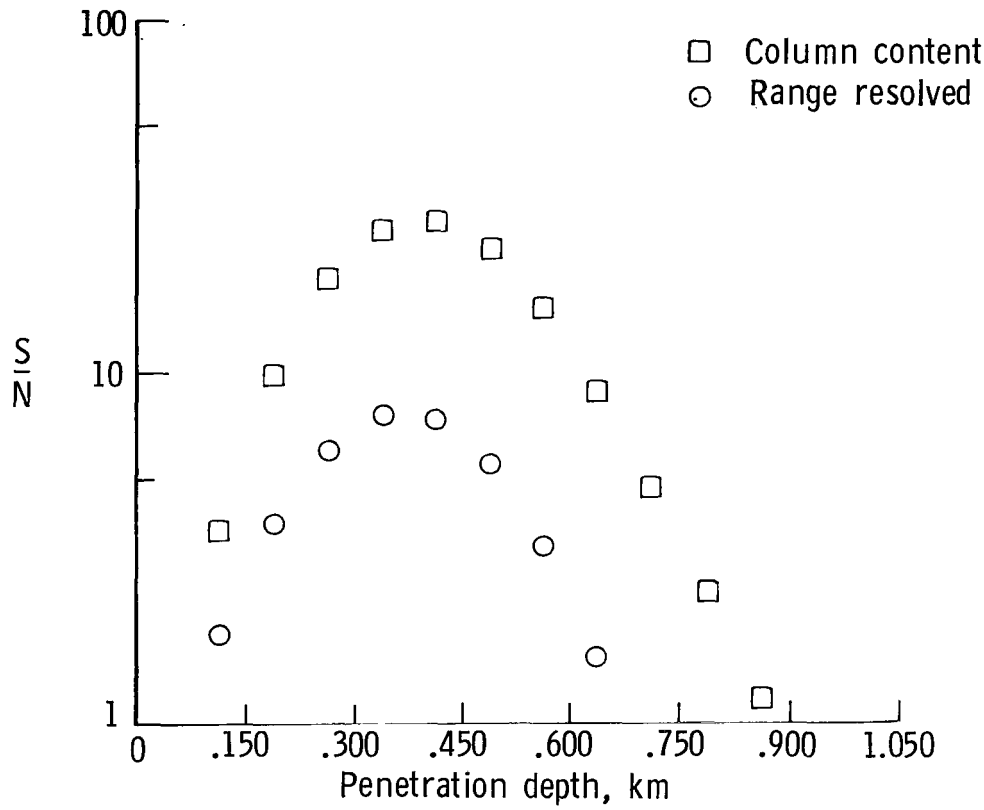

(b) Signal-to-noise ratios as a function of penetration depth.

Figure 10.- Concluded.

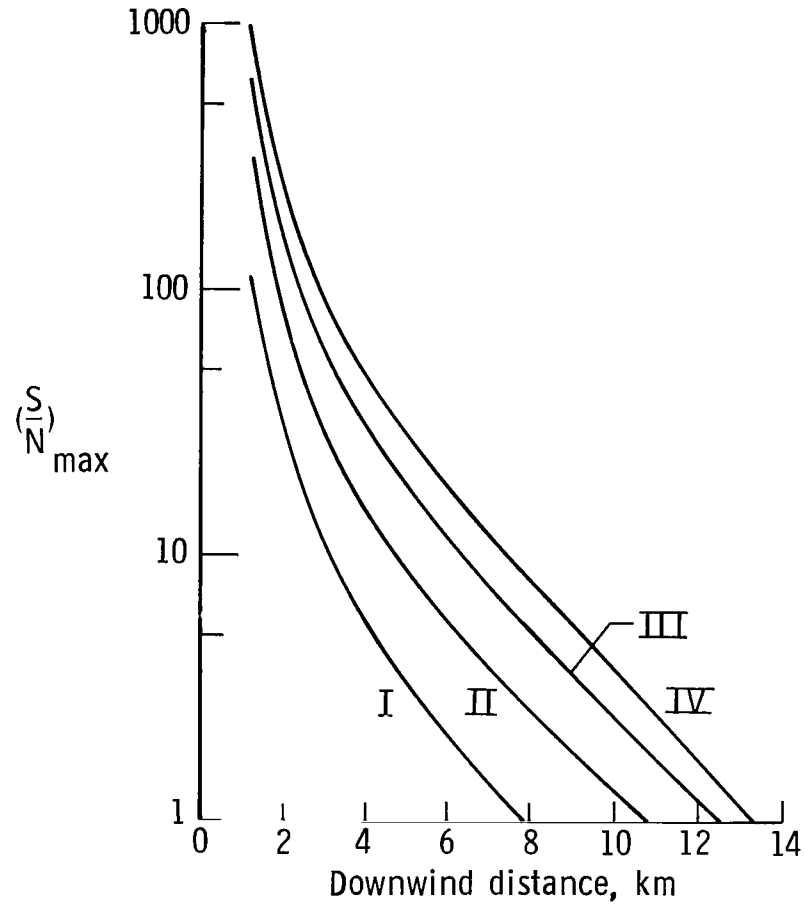

Figure 11.- Maximum S/N as a function of downwind distance for a sea breeze meteorological condition at Kennedy Space Center using H_2O model cloud for four Al_2O_3 models.

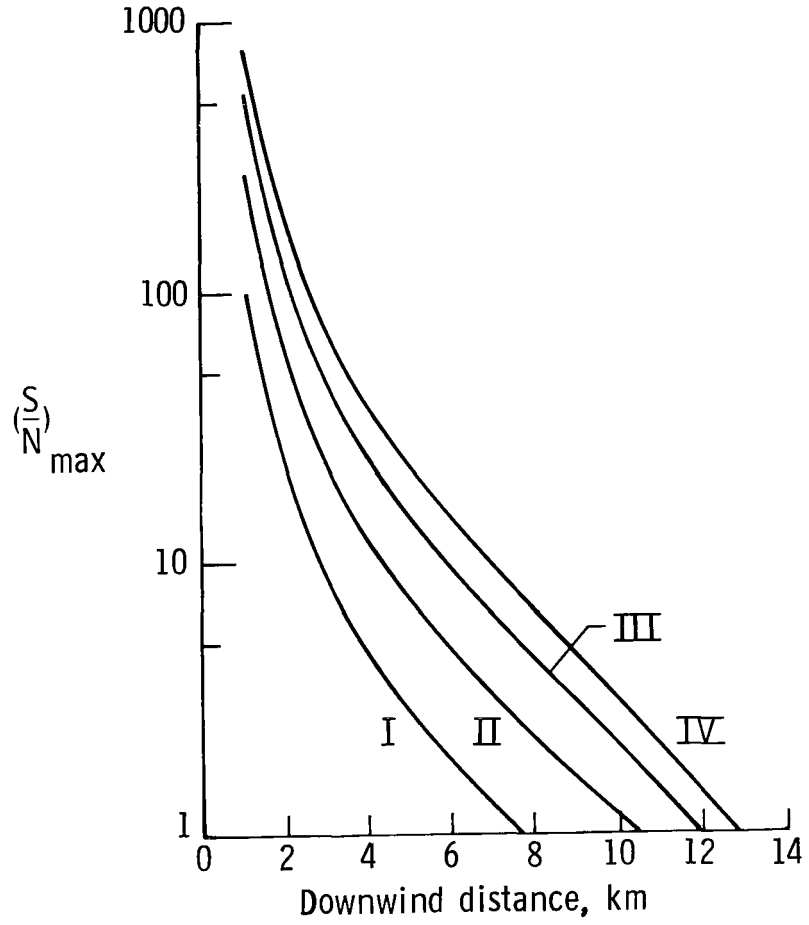

Figure 12.- Maximum S/N as a function of downwind distance for a sea breeze meteorological condition at Kennedy Space Center using H_2O model haze M for four Al_2O_3 models.

NASA-Langley, 1977 L-11144

"The aeronautical and space activities of the United States shall be conducted so as to contribute . . . to the expansion of human knowledge of phenomena in the atmosphere and space. The Administration shall provide for the widest practicable and appropriate dissemination of information concerning its activities and the results thereof."

—NATIONAL AERONAUTICS AND SPACE ACT OF 1958

NASA SCIENTIFIC AND TECHNICAL PUBLICATIONS

TECHNICAL REPORTS: Scientific and technical information considered important, complete, and a lasting contribution to existing knowledge.

TECHNICAL NOTES: Information less broad in scope but nevertheless of importance as a contribution to existing knowledge.

TECHNICAL MEMORANDUMS: Information receiving limited distribution because of preliminary data, security classification, or other reasons. Also includes conference proceedings with either limited or unlimited distribution.

CONTRACTOR REPORTS: Scientific and technical information generated under a NASA contract or grant and considered an important contribution to existing knowledge.

TECHNICAL TRANSLATIONS: Information published in a foreign language considered to merit NASA distribution in English.

SPECIAL PUBLICATIONS: Information derived from or of value to NASA activities. Publications include final reports of major projects, monographs, data compilations, handbooks, sourcebooks, and special bibliographies.

TECHNOLOGY UTILIZATION PUBLICATIONS: Information on technology used by NASA that may be of particular interest in commercial and other non-aerospace applications. Publications include Tech Briefs, Technology Utilization Reports and Technology Surveys.

Details on the availability of these publications may be obtained from:

SCIENTIFIC AND TECHNICAL INFORMATION OFFICE

NATIONAL AERONAUTICS AND SPACE ADMINISTRATION

Washington, D.C. 20546